Effect of interstitial carbon on the evolution of early-stage irradiation damage in equi-atomic FeMnNiCoCr high-entropy alloys

Lu, Eryang

AVS
2020-01-14

Lu , E , Makkonen , I , Mizohata , K , Li , Z , Räisänen , J & Tuomisto , F 2020 , ' Effect of interstitial carbon on the evolution of early-stage irradiation damage in equi-atomic FeMnNiCoCr high-entropy alloys ' , Journal of Applied Physics , vol. 127 , no. 2 , 025103 . https://doi.org/10.1063/1.5

http://hdl.handle.net/10138/313846
10.1063/1.5130748

other
publishedVersion

Journal of Applied Physics

Effect of interstitial carbon on the evolution of early-stage irradiation damage in equi-atomic FeMnNiCoCr high-entropy alloys

Cite as: J. Appl. Phys. **127**, 025103 (2020); https://doi.org/10.1063/1.5130748
Submitted: 09 October 2019 . Accepted: 21 December 2019 . Published Online: 09 January 2020

Eryang Lu, Ilja Makkonen, Kenichiro Mizohata, Zhiming Li, Jyrki Räisänen, and Filip Tuomisto

Journal of Applied Physics ARTICLE scitation.org/journal/jap

Effect of interstitial carbon on the evolution of early-stage irradiation damage in equi-atomic FeMnNiCoCr high-entropy alloys

Cite as: J. Appl. Phys. **127**, 025103 (2020); doi: 10.1063/1.5130748
Submitted: 9 October 2019 · Accepted: 21 December 2019 ·
Published Online: 9 January 2020

Eryang Lu,[1,2,3] Ilja Makkonen,[1,2,4] Kenichiro Mizohata,[2] Zhiming Li,[5,6] Jyrki Räisänen,[2] and Filip Tuomisto[1,2,4]

AFFILIATIONS

[1]Department of Applied Physics, Aalto University, P.O. Box 15100, FI-00076 Espoo, Finland
[2]Department of Physics, University of Helsinki, P.O. Box 43, FI-00014 Helsinki, Finland
[3]Multiple-Research Center, Institute of High Energy Physics, CAS, 100049 Beijing, China
[4]Helsinki Institute of Physics, P.O. Box 64, FI-00014 Helsinki, Finland
[5]Max-Planck-Institut für Eisenforschung, Max-Planck-Straße 1, 40237 Düsseldorf, Germany
[6]School of Materials Science and Engineering, Central South University, 410083 Changsha, China

ABSTRACT

Owing to their excellent radiation tolerance, some of the high-entropy alloys (HEAs) are considered as potential candidates for structural materials in extreme conditions. In order to shed light on the early-stage irradiation damage in HEAs, we performed positron annihilation spectroscopy on hydrogen implanted equiatomic FeMnNiCoCr and interstitial carbon-containing FeMnNiCoCr HEAs. We reveal primary damage as monovacancies in low dose irradiated HEAs. The enhancement of Frenkel pair recombination by C addition is observed in C-containing HEAs. In addition, the C interstitials suppress the vacancy cluster formation in high dose irradiated HEAs.

I. INTRODUCTION

High-entropy alloys (HEAs), or concentrated solid solution alloys (CSSAs), have drawn much research interest over the past few decades.[1–5] Excellent mechanical properties of some HEAs, such as high fracture toughness and ductility at ambient and cryogenic temperatures,[6] and their corrosion and irradiation resistance[4] make them potential materials for hostile conditions. Unlike conventional alloys that usually have one or two prevalent elements, HEAs consist of five or more elements, often in equiatomic compositions, in a single solid solution phase. The chemical complexity induces severe lattice distortion, which subsequently slows down the energy dissipation and further improves the irradiation tolerance.[4–7]

Equiatomic FeMnNiCoCr, first reported by Cantor *et al.*,[1] has been investigated extensively over the past few decades.[7–9] It displays significant suppression of void swelling under irradiation compared to pure nickel.[10] Thermodynamics of vacancies and clusters were also considered in FeMnNiCoCr HEA from theoretical calculations.[11] In spite of considerable research effort, the atomic-scale lattice structure evolution and point defect formation governing the early-stage irradiation damage process are still poorly understood. Residual impurities, such as carbon (C) and nitrogen (N), commonly exist in commercial alloys either as minor alloying elements or low concentration impurities.[12] It has been experimentally confirmed that C atoms interact with point defects, such as vacancies and self-interstitials, in body-centered cubic (bcc) iron.[13,14] Recent studies indicate that C addition improves simultaneously the strength and ductility in FeNiMnAlCr HEAs by increasing the lattice fraction stress.[15] Also, an increase in Vickers hardness was obtained in C-containing FeMnNiCoCr due to the solid solution strengthening as well as the formation of carbides.[16] Li *et al.* reported that the interstitial C addition in nonequiatomic FeMnCoCr HEAs resulted in the joint activation of twinning- and transformation-induced plasticity (TWIP and TRIP) by tuning the matrix phase's instability in a metastable TRIP-assisted dual-phase HEA.[17] Furthermore, a grain refinement has been reported in C-containing cast CrFeCoNi HEAs, and the size of equiaxed grains decreases with increasing C level.[18] In short, minor interstitial C addition improves several of the mechanical properties, for instance, strength, ductility, hardness, and wear resistance in HEAs. In conventional Fe/Ni-based alloys, the interstitial C atoms interact with irradiation vacancies, and the formation of carbon-vacancy

complexes was reported to increase the vacancy migration barriers.[13,19] The irradiation-induced vacancies' migration and aggregation are suppressed due to the stability of C-vacancy complexes with varying sizes.[20]

In the present study, the physical processes of early-stage irradiation damage (≤1 dpa) and point defects' evolution in equiatomic FeMnNiCoCr HEAs with and without C addition are characterized by positron annihilation spectroscopy (PAS). The effects of interstitial C atoms on primary damage formation and evolution are systematically studied in interstitial HEAs (iHEAs) with varying C contents.

II. EXPERIMENT AND MODELING

A. Samples and preparation

The face-centered cubic (fcc) structured equimolar FeMnNiCoCr and interstitial C soluted iHEAs ingots with nominal composition $FeMnNiCoCrC_x$ ($x = 0.2$, 0.5, 0.8 at. %) were synthesized in a vacuum induction furnace by arc melting using pure metals and carbon. The original cast was subsequently hot rolled at 950 °C to a thickness reduction of 50%. The exact carbon concentrations in the three iHEAs were identified as 0.25, 0.53, and 0.9 (at. %), respectively, by wet-chemical analysis.[21] All specimens were homogenized at 1200 °C for 3 h in the Ar atmosphere followed by water-quenching (WQ). The compositional homogeneity of the various HEA samples at the microscale was verified by energy-dispersive X-ray spectroscopy. The averaged grain size of ~200 μm was obtained from all of the homogenized alloys. Further details on the mechanical properties and characterization can be seen in Ref. 21. Sheet specimens with dimensions of $5 \times 5 \times 0.5$ mm^3 were machined from the WQ alloys. Mechanical polishing with the SiC paper followed by the colloidal silica suspension with 40 nm particles was performed on sample surfaces to obtain a mirrorlike finish. An electrochemical method was utilized to remove the subsurface damage layer from the mechanical polishing process by low temperature (−30 °C) etching.

B. Hydrogen ion implantation

The distribution of irradiation damage and implantation profiles of 150 keV hydrogen in equiatomic FeMnNiCoCr HEA with C addition was calculated by SRIM-2013.[22] The average displacement thresholds were set as 40 eV for each element. The results are shown in Fig. 1, which indicates that the irradiation damage accumulates and peaks at around 600 nm. Furthermore, three different depth layers were identified based on the SRIM calculation: track layer (L1), damage layer (L2), and nonirradiated layer (L3). The implanted ions pass through L1 by the electronic energy loss process, producing mainly primary-knock-induced Frenkel pairs (monovacancy + self-interstitial). The radiation damage accumulates and the implanted ions stop by cascade collisions with lattice atoms in L2, and there is no energy dissipation or ion deposition in L3.[23]

The surface prepared specimens were irradiated with 300 keV H_2^+ ions (150 keV H^+ ions) at room temperature using the 500-kV ion implanter at the University of Helsinki. The implantation fluence φ ranged from 2.5×10^{14} ions/cm^2 up to 2.5×10^{17} ions/cm^2. The ion beam swept for homogenous exposure over a 10×10 cm^2 square implantation area. All samples were mounted on aluminum plates coupled with 15 cm diameter and an ion flux of 5×10^{12} atoms/cm^2/s, which suppressed overheating of the samples.

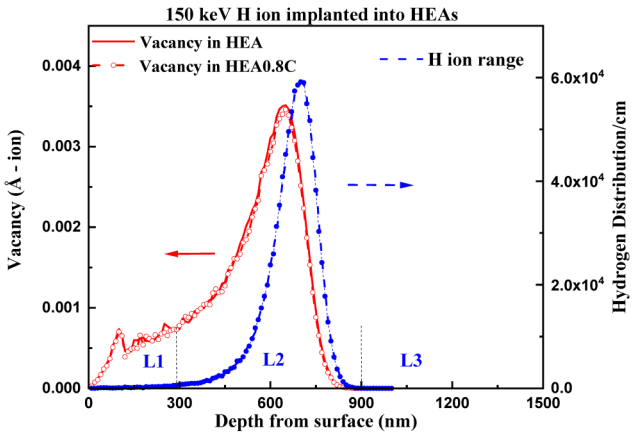

FIG. 1. SRIM calculation showing the irradiation damage and implanted atom deposition of 150 keV hydrogen ions in equiatomic FeMnNiCoCr and FeMnNiCoCr + (0.8 at. %) C HEAs.

C. Positron annihilation spectroscopy

Positron annihilation spectroscopy (PAS) is a unique and sensitive probe to lattice defects with limited concentration.[24,25] Earlier work with PAS on single phase fcc HEA[8] and concentrated solid solution alloys[26,27] highlights the importance of performing systematic studies with several irradiation doses and alloy composition. In this work, we employed positron annihilation spectroscopy to characterize the microstructural evolution through vacancy-type defects in the irradiated samples. We performed positron lifetime experiments in virgin (un-irradiated) samples with a standard digital spectrometer in collinear geometry and a time resolution of 240 ps. We performed the conventional Doppler broadening measurements of positron annihilation radiation with a variable-energy positron beam (positron energy range from 0.5 keV to 35 keV). We used high purity germanium (HPGe) detectors with an energy resolution of 1.2 keV at 511 keV. The integration windows for the conventional S and W parameters describing the shape of the Doppler broadened annihilation line were set to ($|P_L| < 0.4$ a.u.) and (1.6 a.u. $< |P_L| <$ 4.0 a.u.), respectively. More details on the experimental techniques and data analysis can be found in Refs. 24 and 25.

The average positron lifetime in all virgin samples was found to be between 116 ps and 119 ps, close to the bulk lifetime of the nickel matrix (110 ps)[28] and the defect-free positron lifetime (112 ps) as assigned in equiatomic CoCrFeMnNi.[8] This indicates that the virgin samples have low concentrations of vacancy defects and that these samples can be used as a good reference point for defect studies. The Doppler broadening parameters obtained far away from the surface in the virgin samples vary in a narrow range $S = 0.411$–0.415 and $W = 0.080$–0.082, similarly as the average

lifetimes. The effective positron diffusion lengths were estimated to be around 100 nm in all virgin samples by VEPFIT analysis.[29]

D. Theoretical calculations

First-principles calculations employing the two-component electron-positron density functional theory[30] were performed to predict the positron states and annihilation parameters in the bulk and at defects. Cubic $2 \times 2 \times 2$ supercells with 32 atoms were constructed for the fcc elemental solids of Cr, Mn, Fe, Co, and Ni. The plane-wave cut-off energy was fixed to 300 eV, and a $6 \times 6 \times 6$ Monkhorst-Pack k mesh[31] was used for all systems. We employed the projector augmented wave (PAW) method[32] as implemented in the Vienna *Ab initio* Simulation Package (VASP) code[33–35] and the generalized-gradient approximation[36] for electron exchange and correlation energy. We used the local-density approximation[31] for the electron-positron correlation potential and enhancement factor. The positron modeling was performed in the approximation, in which the positron does not affect the average electron density, and we took the zero-positron-density limits of the appropriate functionals.[31] Due to certain compensation and feedback mechanisms, this approach has been shown to provide results that are consistent with more self-consistent modeling.[37] All of the vacancy supercells were fully relaxed including repulsive forces on ions due to the localized positron.

The momentum distribution of annihilating pairs was calculated using the so-called state-dependent model[38] and the PAW method.[39,40] The computational Doppler spectra were first convoluted with the experimental resolution function, and the relative *S* and *W* parameters were extracted for all models and defined relative to bulk Ni. The computational *S* and *W* parameters of a vacancy-free equiatomic FeMnNiCoCr HEA were obtained through averaging the *S* and *W* parameters calculated for the elemental fcc metal systems of Fe, Mn, Ni, Co, and Cr with equal weights. The same averaging procedure was used separately for mono-, di-, and tetravacancies. It has been shown that in the close-packed fcc structure, the spectrum of a vacancy defect decorated by alloying elements can be reproduced using a weighted average of vacancy spectra calculated for the constituent elemental metals.[41] In the present case, all the lattice structures can even be assumed the same, namely, fcc with almost equal lattice parameters.

III. RESULTS AND ANALYSIS

A. C-free HEA

Figure 2(a) shows the *S*-*E* curve of the virgin HEA, suggesting that the S parameter decreases with increasing energy from the surface and saturates at a value of 0.412. The *S* parameters are large compared to that of the virgin sample already at the damage level of 1×10^{-3} dpa, demonstrating generation of vacancy-type defects due to irradiation. The *S* parameters are rather constant in L1 and increase when the detection depth reaches L2. The maxima of *S*-*E* curves occur between 400 nm and 600 nm from the surface, which are located within L2 for all irradiated HEAs, consistent with the SRIM calculation. At higher positron implantation energies, the *S* parameters gradually approach the virgin HEA value due to the broadening of the implantation profile with increasing positron energy.

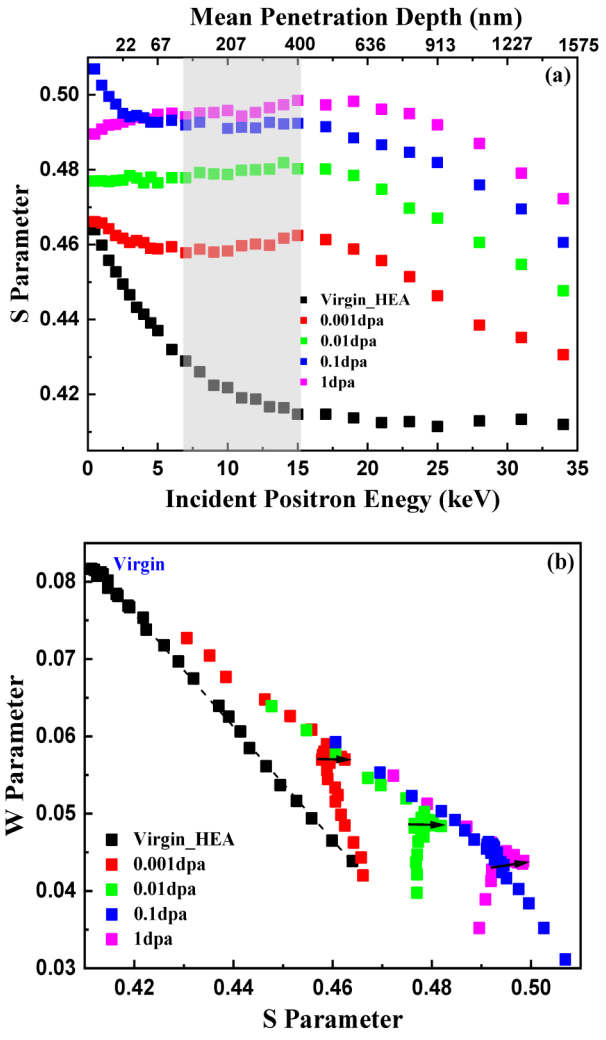

FIG. 2. Doppler broadening data of hydrogen-irradiated C-free HEAs. (a) *S*-*E* curves with the mean penetration depth of positrons on the top axis. The variation of *S* parameters from L1 to L2 takes place within the gray area; (b) (*S*, *W*) plot. Error bars are smaller than the size of markers.

The (*S*, *W*) data in irradiated HEAs with different damage levels are shown in Fig. 2(b) with the implantation energy as a running parameter. The (*S*, *W*) plot of virgin samples displays a straight line, indicating that the electrochemical polishing procedure effectively removes subsurface damage in samples. Compared to the virgin sample, the (*S*, *W*) points of irradiated HEAs are located toward the lower right, as is typical for vacancy-type defects. All of the (*S*, *W*) points approach the virgin state at the highest implantation energies in the L3 layer. The small arrows in Fig. 2(b) show the evolution of the (*S*, *W*) data points from L1 to L2 layers in the irradiated solids. Lines connecting the bulk point to the data points in L1 and L2 have different slopes, indicating that the nature of the damage is different at these depths.

B. C-containing iHEAs

Figures 3(a)–3(d) illustrate the radiation damage accumulation and microdefect evolution in iHEAs with different C contents (0, 0.2, 0.5, and 0.8 at. %).

In Fig. 3(a), the *S*-*E* curves of C-free HEA and HEA0.2C are essentially identical, indicating similar defect evolution in the lowest-dose irradiated samples. The *S* parameters increase less with irradiation in the samples with a higher content of carbon interstitials, indicating the suppression of irradiation damage, either in terms of the concentration or of the size of vacancy defects. Also, the maxima of the *S*-*E* plots are found less pronounced in the iHEAs with higher C content.

The *S*-*E* curves in 0.01 dpa irradiated samples are shown in Fig. 3(b). As in the case of the lowest dose irradiation, the *S*-*E* curves are essentially identical for C-free HEA and HEA0.2C. With more C in the alloy, the *S* parameters are lower with the same irradiation condition in both L1 and L2, but the difference is less pronounced than for the lowest dose irradiation. In contrast to the lowest dose, the shape of the *S*-*E* curves is the same for all the samples.

The *S*-*E* curves of 0.1 and 1 dpa irradiated samples are shown in Figs. 3(c) and 3(d), respectively. After 0.1 dpa irradiation, the *S* parameters at L1 and L2 in HEA0.2C increase less than that in C-free HEA. In the samples with higher C content, the irradiation-induced increase of the *S* parameter is further suppressed, which highlights the effect of C addition on radiation damage suppression in HEAs. The *S*-*E* curves of 0.1 dpa irradiated HEA0.5C and HEA0.8C now overlap, while they were clearly different with lower doses. As the irradiation damage increases up to 1 dpa, the increment of *S* parameters in HEAs with the C content between 0.2 and 0.8 is essentially the same in L1, and the result is clearly different from C-free HEA.

C. Identification of the irradiation-induced vacancy defects

The variation of (*S*, *W*) parameters from the layer L1–L2 in irradiated HEAs is shown in Fig. 4. The relative (*S*, *W*) parameters of monovacancy (V1), divacancy (V2), and vacancy clusters (V4) from calculations are shown in the inset. The scales of the relative

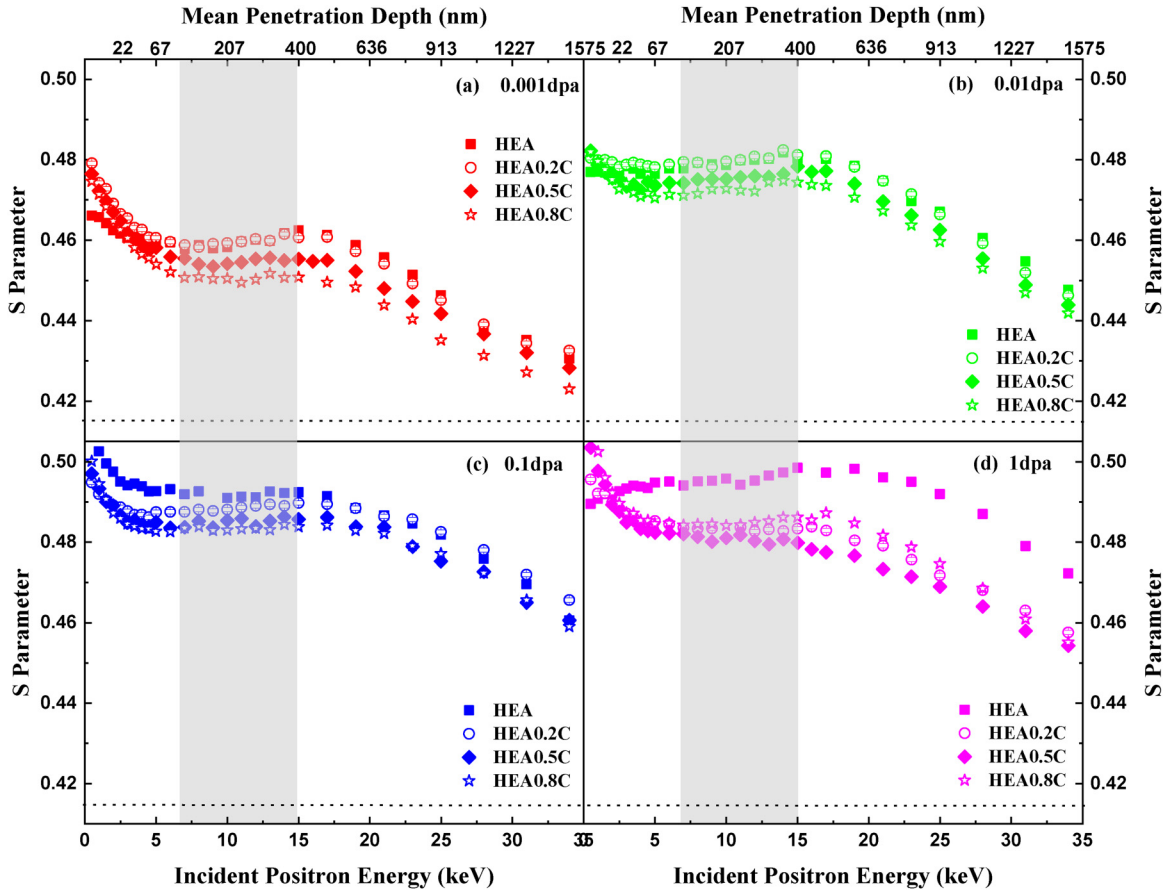

FIG. 3. *S*-*E* curves of hydrogen-irradiated C-containing FeMnNiCoCr iHEAs. The dotted line displays the *S* values of virgin samples. The *S*-*E* curves are divided to 4 subfigures with increasing irradiation damage level: (a) 0.001 dpa, (b) 0.01 dpa, (c) 0.1 dpa, and (d) 1 dpa. The variation of *S* parameters from L1 to L2 takes place within the gray area. Error bars are smaller than the size of markers.

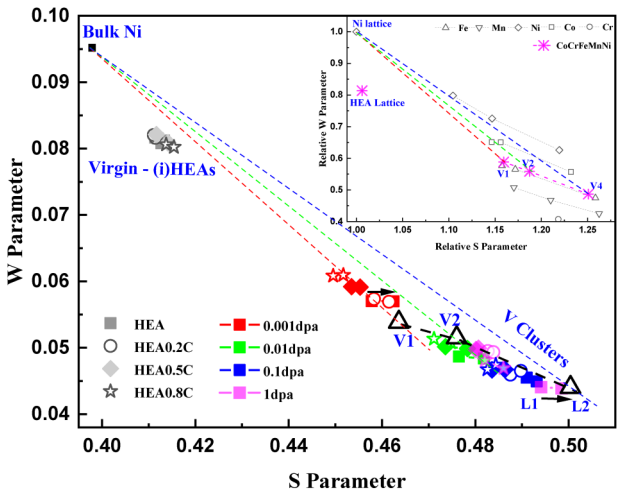

FIG. 4. The experimental (*S*, *W*) parameters in the HEA samples are shown in the main part of the figure, and the black arrows indicate the (*S*, *W*) evolution from L1 to L2 in irradiated samples. The inset shows the calculated relative *S* and *W* parameters of different vacancy states, which are normalized to the Ni lattice values. The dashed lines between the Ni lattice and monovacancy (V1), divacancy (V2) or 4-vacancy cluster (V4) are the same in the inset and in the main figure. Error bars are not shown as they are smaller than the size of the markers.

parameters in the inset and the absolute parameters in the figure itself are comparable. In the main figure, the computational data are scaled in such a way that the bulk Ni reference point coincides with the computational Ni lattice point, and the computational (*S*, *W*) points of different vacancy states are shown as large hollow triangles. The (*S*, *W*) points of all virgin samples are the same regardless of the C content. The (*S*, *W*) points from L1 to L2 of 0.001 dpa irradiated samples are displayed using the red markers. The (*S*, *W*) points of 0.001 dpa irradiated samples in the track layer (L1) are located on the V1 line regardless of C content, while the defect type in the damage layer (L2) varies as the C content is increased. Vacancy defects larger than V1 are clearly detected in C-free HEA and HEA0.2C, while V1 is the dominant defect type in higher C-containing iHEAs. As the irradiation damage level is increased up to 0.01 dpa, the variation of (*S*, *W*) points from L1 to L2 is marked by green labels. Here, all 4 samples have their L1 and L2 points on the same respective lines, with the L1 data between V1 and V2 and the L2 data coinciding with the V2 line. This indicates that the vacancy sizes are similar in all the samples irradiated at 0.01 dpa, and only the vacancy concentrations decrease when the C content increases above 0.2% (the data for C-free HEA and HEA0.2C coincide). When going from the 0.001 dpa irradiation to 0.01 dpa irradiation, the (*S*, *W*) data move mostly along the V1 (and V2) lines, indicating that positrons detect an increase in the vacancy concentration in addition to the increase in the vacancy sizes.

The experimental data for 0.1 dpa irradiated samples from L1 and L2 are marked by blue symbols. The (*S*, *W*) points hardly change from L1 to L2, and they are all located between the V2 and V cluster lines. There is a clear shift of the data points toward the V2 line with increasing C content, and the C-free HEA and HEA0.2C data points no longer coincide. When going from the 0.01 dpa irradiation to 0.1 dpa irradiation, the data points move parallel to the V1–V2–V4 point evolution (rather than along one of the V1, V2, or V4 lines), indicating that positrons no longer detect an increase in the vacancy concentrations. This means that the positron trapping at vacancy defects has reached saturation after 0.01 dpa irradiation; i.e., all positrons annihilate as they are trapped at vacancy defects, and further concentration increases cannot be observed. The experimental data for 1 dpa irradiated samples are marked with purple symbols. The (*S*, *W*) data of C-free HEA continue shifting toward the larger vacancy cluster values, with a distinct difference between L1 and L2 (defects are larger in L2), while the data for the HEA0.5C and HEA0.8C samples hardly change from the 0.1 dpa irradiation. Now, the HEA0.2C sample data essentially coincide with those of the samples with higher C content.

IV. DISCUSSION

The observation that the positron data are in saturation after 0.01 dpa irradiation but not after 0.001 dpa irradiation and that the (*S*, *W*) data are already close to the theoretical V1 point in Fig. 4 allows us to estimate the monovacancy concentration and hence the monovacancy introduction rate (primary damage) due to electronic stopping in L1. The positron trapping rate is proportional to the defect concentration as $\kappa_V = \mu_V C_d$, where μ_V is the positron trapping coefficient and C_d is the defect concentration. Estimating that the positron trapping fraction (η) at monovacancies is 90% after 0.001 dpa irradiation in C-free HEA and assuming a bulk HEA lifetime (τ_B) of 110 ps and employing the solution to the kinetic positron trapping model where $\eta = \kappa_V/(\lambda_B + \kappa_V)$, we obtain a positron trapping rate at monovacancies of $\kappa_V = 8.2 \times 10^{10}\ s^{-1}$.[42] Assuming a monovacancy positron trapping coefficient of $\mu_V = 5 \times 10^{14}\ s^{-1}$ typical of metals,[43–45] this translates into a vacancy concentration of 160 ppm or $[V] = 1.5 \times 10^{19}\ cm^{-3}$. The introduction rate for monovacancies at 0.001 dpa (fluence $\phi = 2.5 \times 10^{14}\ cm^{-2}$) is hence $\Sigma = [V]/\varphi = 6 \times 10^4\ cm^{-1}$, agreeing very well with the values predicted by SRIM that vary from $5 \times 10^4\ cm^{-1}$ to $7 \times 10^4\ cm^{-1}$ in L1 (see Fig. 1). It indicates that the monovacancies observed in the C-free HEA are indeed the primary damage, and very little effect from Frenkel pair recombination is present, suggesting that the monovacancy defects are not very mobile at RT in HEA or that they are stabilized in the crystal instead of diffusing out through the surface. The self-interstitials produced in the irradiation also need to be efficiently trapped elsewhere in the crystal instead of recombining with the monovacancies. In addition, the implanted hydrogen should not play a role in L1.

Two different C-related phenomena governing the early-stage irradiation defect formation and evolution can be observed in the positron data. First, at low damage levels, that is, on the ion track (L1) after 0.001 and 0.01 dpa irradiation, the presence of a sufficiently high content (0.5 at. % or more) of C appears to reduce the introduction rate of primary damage, manifested through lower vacancy concentrations. Second, an even more pronounced effect as it is observed in all C-containing HEAs is that the mere presence of carbon in the HEA matrix suppresses the formation of larger

vacancy clusters when significant amounts of damage are accumulated (0.1 and 1 dpa). The suppression of vacancy clustering at high C content is seen also in the lower-dose samples in the implantation damage zone (L2). We discuss these two phenomena in more detail in the following.

A. Carbon-induced suppression of vacancy cluster formation

Earlier research has shown that stable carbon-vacancy (C-V) complexes are easily formed in Fe and Ni based alloys.[13,20,43] The migration barriers of C-V complexes are higher than those of isolated vacancies, and the self-diffusivity of vacancy defects is also suppressed by increasing the C content in bcc Fe.[46] Theoretical calculations suggest that a vacancy can bind up to two C atoms in bcc Fe.[47] The binding energy of the C-V complex was calculated as 0.58 eV with the vacancy migration energy of 0.55 eV, and the binding energy increased up to 0.61 eV for the C_2-V complex in Fe-C systems. The binding energy of C atoms in C_4-V_2 clusters raised up to 0.93 eV in the same system.[48] Similar work performed for austenitic steel and fcc Ni also predicts that a vacancy can stably bind up to two C atoms with the binding energy up to 0.4 eV in austenitic steel and 0.1 eV in Ni per solute atom.[12] In all the C-containing iHEAs, the C content (2000 ppm–8000 ppm) is clearly higher than that required for saturation trapping of positrons (~100 ppm), while the amount of primary damage is of the order of 10^6 ppm (1 dpa). Hence, C interstitials are likely to be efficient trapping sites for irradiation-induced vacancies, given that the concentrations of both are high enough. Efficient trapping of irradiation-induced vacancies by C interstitials limits the clustering process, observed as smaller clusters in high-damage iHEAs. It should be noted that hydrogen is likely to be involved in the vacancy clusters also in some way; however, the effect of hydrogen on the positron signals in the case of vacancy clusters is minor. In any case, there should be no difference between C-free HEA and C-containing iHEAs.

B. Carbon-induced suppression of primary damage at low doses

Due to the low damage cross section at the track layer (L1), primary-knock-induced monovacancy formation governs the microstructural evolution at the early-stage irradiation process (<0.01 dpa). The primary damage at low doses appears to stick, and no Frenkel pair recombination is present. Vacancy out-diffusion does not take place either, based on the concentration of irradiation-induced vacancies as discussed above. It is clearly seen that 0.2 at. % C addition is not enough to make a difference in primary damaged HEA. However, 0.5 and 0.8 at. % C addition causes an apparent reduction of monovacancy concentration in L1. Hydrogen is not involved in defect evolution in L1 as the amount of implanted ions deposited in L1 is very limited. Carbon-vacancy (C-V) complex formation also should not be the main effect since no visible suppression of primary damage is observed in HEA0.2C, whose C content is one order of magnitude higher than that in the C-free HEA. Theoretical calculations on the interactions of foreign interstitial atoms (C, N) with point defects in bcc Fe suggest that strong binding energy exists between C interstitials and a vacancy, whereas a repulsion is observed between C atoms and self-interstitial atoms.[47] Hence, another mechanism needs to be considered. We propose that the presence of interstitial C in high concentrations blocks the potential trapping sites for self-interstitials atoms (SIAs), hence allowing the SIAs fall back into the vacancies (Frenkel pair recombination) more efficiently. This explanation assumes that the concentration of potential traps for any kind of interstitials is between 0.2 and 0.5 at. %, This blocking of potential traps for SIAs, together with the repulsion between C interstitials and SIAs, can also enhance SIA diffusion and subsequently increase the probability of recombination with vacancies.

V. CONCLUSION

We have performed positron annihilation experiments on hydrogen implanted equiatomic FeMnNiCoCr and C-containing FeMnNiCoCr high-entropy alloys in order to understand the early-stage irradiation damage process. Primary damage (monovacancies) in the track layer of low dose irradiated C-free HEA is observed with limited Frenkel pair recombination. The presence of interstitial C in iHEA blocks the traps for self-interstitial atoms with the repulsion mechanism and enhances the Frenkel pair recombination, which limits the primary damage formation in low dose irradiated C-containing iHEAs when the C content is sufficiently high (e.g., ≥0.5%). Efficient trapping of irradiation-induced vacancies by C interstitials limits the vacancy clustering process and results in smaller clusters accumulating in high dose irradiated C-containing iHEAs. The C interstitials suppress the irradiation-induced primary damage formation and vacancy clustering and thus improve the irradiation tolerance of HEAs.

ACKNOWLEDGMENTS

This work was supported by the Helsinki Institute of Physics Technology Programme, the Academy of Finland (Project Nos. 285809, 293932, and 319178), and the International Postdoctoral Exchange Fellowship Program (No. 20170071) by the Office of China Postdoctoral Council. CSC—IT Center for Science, Finland, is acknowledged for providing the computational resources.

REFERENCES

[1]B. Cantor, I. T. H. Chang, P. Knight, and A. J. B. Vincent, Mater. Sci. Eng. A **375–377**, 213 (2004).
[2]D. B. Miracle and O. N. Senkov, Acta Mater. **122**, 448 (2017).
[3]J.-W. Yeh, S.-K. Chen, S.-J. Lin, J.-Y. Gan, T.-S. Chin, T.-T. Shun, C.-H. Tsau, and S.-Y. Chang, Adv. Eng. Mater. **6**, 299 (2004).
[4]Y. Zhang, G. M. Stocks, K. Jin, C. Lu, H. Bei, B. C. Sales, L. Wang, L. K. Béland, R. E. Stoller, G. D. Samolyuk, M. Caro, A. Caro, and W. J. Weber, Nat. Commun. **6**, 8736 (2015).
[5]Z. Li, K. G. Pradeep, Y. Deng, D. Raabe, and C. C. Tasan, Nature **534**, 227 (2016).
[6]B. Gludovatz, A. Hohenwarter, D. Catoor, E. H. Chang, E. P. George, and R. O. Ritchie, Science **345**, 1153 (2014).
[7]H.-S. Do and B.-J. Lee, Sci. Rep. **8**, 16015 (2018).
[8]M. Elsayed, R. Krause-Rehberg, C. Eisenschmidt, N. Eißmann, and B. Kieback, Phys. Status Solidi Appl. Mater. Sci. **215**, 1800036 (2018).
[9]F. Zhang, Y. Tong, K. Jin, H. Bei, W. J. Weber, A. Huq, A. Lanzirotti, M. Newville, D. C. Pagan, J. Y. P. Ko, and Y. Zhang, Mater. Res. Lett. **6**, 450 (2018).

[10]C. Lu, L. Niu, N. Chen, K. Jin, T. Yang, P. Xiu, Y. Zhang, F. Gao, H. Bei, S. Shi, M. R. He, I. M. Robertson, W. J. Weber, and L. Wang, Nat. Commun. **7**, 13564 (2016).
[11]Z. Wang, C. T. Liu, and P. Dou, Phys. Rev. Mater. **1**, 043601 (2017).
[12]D. J. Hepburn, D. Ferguson, S. Gardner, and G. J. Ackland, Phys. Rev. B **88**, 024115 (2013).
[13]P. Hautojärvi, J. Johansson, A. Vehanen, J. Yli-Kauppila, and P. Moser, Phys. Rev. Lett. **44**, 1326 (1980).
[14]A. Vehanen, P. Hautojärvi, J. Johansson, J. Yli-Kauppila, and P. Moser, Phys. Rev. B **25**, 762 (1982).
[15]Z. Wang, I. Baker, Z. Cai, S. Chen, J. D. Poplawsky, and W. Guo, Acta Mater. **120**, 228 (2016).
[16]N. D. Stepanov, N. Y. Yurchenko, M. A. Tikhonovsky, and G. A. Salishchev, J. Alloys Compd. **687**, 59 (2016).
[17]Z. Li, C. C. Tasan, H. Springer, B. Gault, and D. Raabe, Sci. Rep. **7**, 40704 (2017).
[18]X. W. Liu, L. Liu, G. Liu, X. X. Wu, D. H. Lu, J. Q. Yao, W. M. Jiang, Z. T. Fan, and W. B. Zhang, Metall. Mater. Trans. A **49**, 2151 (2018).
[19]A. P. Druzhkov, D. A. Perminov, and V. L. Arbuzov, J. Nucl. Mater. **430**, 279 (2012).
[20]D. Terentyev, K. Heinola, A. Bakaev, and E. E. Zhurkin, Scr. Mater. **86**, 9 (2014).
[21]Z. Li, Acta Mater. **164**, 400 (2019).
[22]R. E. Stoller, M. B. Toloczko, G. S. Was, A. G. Certain, S. Dwaraknath, and F. A. Garner, Nucl. Instrum. Methods Phys. Res. Sect. B **310**, 75 (2013).
[23]A. Debelle, M. F. Barthe, and T. Sauvage, J. Nucl. Mater. **376**, 216 (2008).
[24]F. Tuomisto and I. Makkonen, Rev. Mod. Phys. **85**, 1583 (2013).
[25]J. Čížek, J. Mater. Sci. Technol. **34**, 577 (2018).
[26]S. Abhaya, R. Rajaraman, S. Kalavathi, and G. Amarendra, J. Alloys Compd. **620**, 277 (2015).
[27]S. Abhaya, R. Rajaraman, S. Kalavathi, C. David, B. K. Panigrahi, and G. Amarendra, J. Alloys Compd. **669**, 117 (2016).
[28]E. Kuramoto, T. Tsutsumi, K. Ueno, M. Ohmura, and Y. Kamimura, Comput. Mater. Sci. **14**, 28 (1999).
[29]A. van Veen, H. Schut, M. Clement, J. M. M. de Nijs, A. Kruseman, and M. R. IJpma, Appl. Surf. Sci. **85**, 216 (1995).
[30]E. Boronski and R. M. Nieminen, Phys. Rev. B **34**, 3820 (1986).
[31]H. J. Monkhorst and J. D. Pack, Phys. Rev. B **13**(12), 5188 (1976).
[32]P. E. Blöchl, Phys. Rev. B **50**, 17953 (1994).
[33]G. Kresse and J. Furthmüller, Comput. Mater. Sci. **6**, 15 (1996).
[34]G. Kresse and J. Furthmüller, Phys. Rev. B: Condens. Matter Mater. Phys. **54**, 11169 (1996).
[35]G. Kresse and D. Joubert, Phys. Rev. B **59**, 1758 (1999).
[36]J. P. Perdew, K. Burke, and M. Ernzerhof, Phys. Rev. Lett. **77**, 3865 (1996).
[37]M. J. Puska, A. P. Seitsonen, and R. M. Nieminen, Phys. Rev. B **52**, 10947 (1995).
[38]M. Alatalo, B. Barbiellini, M. Hakala, H. Kauppinen, T. Korhonen, M. Puska, K. Saarinen, P. Hautojärvi, and R. Nieminen, Phys. Rev. B: Condens. Matter Mater. Phys. **54**, 2397 (1996).
[39]I. Makkonen, M. Hakala, and M. J. Puska, J. Phys. Chem. Solids **66**, 1128 (2005).
[40]I. Makkonen, M. Hakala, and M. J. Puska, Phys. Rev. B: Condens. Matter Mater. Phys. **73**, 035103 (2006).
[41]P. Folegati, I. Makkonen, R. Ferragut, and M. J. Puska, Phys. Rev. B: Condens. Matter Mater. Phys. **75**, 054201 (2007).
[42]P. Hautojärvi and C. Corbel, "Positron spectroscopy of defects in metals and semiconductors," in *Positron Spectroscopy of Solids* (IOS Press, Amsterdam, 1995).
[43]J. Wolffs, M. Franz, J. Kluin, and D. Schmid, Acta Mater. **45**, 4759 (1997).
[44]M. J. Puska and R. M. Nieminen, J. Phys. F: Met. Phys. **17**, 2235 (1987).
[45]J. Dryzek, J. Phys. Condens. Matter **7**, L383 (1995).
[46]M. Kabir, T. T. Lau, X. Lin, S. Yip, and K. J. Van Vliet, Phys. Rev. B: Condens. Matter Mater. Phys. **82**, 134112 (2010).
[47]C. Domain, C. S. Becquart, and J. Foct, Phys. Rev. B: Condens. Matter Mater. Phys. **69**, 144112 (2004).
[48]M. J. Konstantinović and L. Malerba, Phys. Rev. Mater. **1**, 053602 (2017).